
HIERARCHICAL SEVERITY STAGING OF ANTERIOR CRUCIATE LIGAMENT INJURIES USING DEEP LEARNING

Nikan K Namiri

Center for Intelligent Imaging
Department of Radiology and Biomedical Imaging
University of California, San Francisco
San Francisco, CA 94107

Io Flament

Center for Intelligent Imaging
Department of Radiology and Biomedical Imaging
University of California, San Francisco
San Francisco, CA 94107

Bruno Astuto

Center for Intelligent Imaging
Department of Radiology and Biomedical Imaging
University of California, San Francisco
San Francisco, CA 94107

Rutwik Shah

Center for Intelligent Imaging
Department of Radiology and Biomedical Imaging
University of California, San Francisco
San Francisco, CA 94107

Radhika Tibrewala

Center for Intelligent Imaging
Department of Radiology and Biomedical Imaging
University of California, San Francisco
San Francisco, CA 94107

Francesco Caliva

Center for Intelligent Imaging
Department of Radiology and Biomedical Imaging
University of California, San Francisco
San Francisco, CA 94107

Thomas M Link

Center for Intelligent Imaging
Department of Radiology and Biomedical Imaging
University of California, San Francisco
San Francisco, CA 94107

Valentina Pedita

Center for Intelligent Imaging
Department of Radiology and Biomedical Imaging
University of California, San Francisco
San Francisco, CA 94107

Sharmila Majumdar

Center for Intelligent Imaging
Department of Radiology and Biomedical Imaging
University of California, San Francisco
San Francisco, CA 94107
Sharmila.Majumdar@ucsf.edu

March 23, 2020

Note: This work has been submitted to Radiology: Artificial Intelligence for possible publication. Copyright may be transferred without notice, after which this version may no longer be accessible.

ABSTRACT

Purpose: To evaluate diagnostic utility of two convolutional neural networks (CNNs) for severity staging anterior cruciate ligament (ACL) injuries.

Materials and Methods: This retrospective analysis was conducted on 1243 knee MR images (1008 intact, 18 partially torn, 77 fully torn, 140 reconstructed ACLs) from 224 subjects collected between 2011 and 2014 (age=46.50±13.55 years, body mass index=24.58±3.60 kg/m², 46% women (mean±standard deviation)). Images were acquired with a 3.0T MR scanner using 3D fast spin echo CUBE-

sequences. The radiologists used a modified scoring metric analogous to the ACLOAS and WORMS for grading standard. To classify ACL injuries with deep learning, two types of CNNs were used, one with three-dimensional (3D) and the other with two-dimensional (2D) convolutional kernels. Performance metrics included sensitivity, specificity, weighted Cohen’s kappa, and overall accuracy, followed by two-sample t-tests to compare CNN performance.

Results: The overall accuracy (84%) and weighted Cohen’s kappa (.92) reported for ACL injury classification were higher using the 2D CNN than the 3D CNN. The 2D CNN and 3D CNN performed similarly in assessing intact ACLs (2D CNN: 93% sensitivity and 90% specificity, 3D CNN: 89% sensitivity and 88% specificity). Classification of full tears by both networks were also comparable (2D CNN: 83% sensitivity and 94% specificity, 3D CNN: 77% sensitivity and 100% sensitivity). The 2D CNN classified all reconstructed ACLs correctly.

Conclusion: CNNs applied to ACL lesion classification results in high sensitivity and specificity, leading to potential use in helping grade ACL injuries by non-experts.

1 Introduction

The anterior cruciate ligament (ACL) is the most commonly injured ligament in the knee (1,2). ACL injuries increase the risk of developing posttraumatic knee osteoarthritis (OA) and total knee replacement (3–6). MRI is currently the most effective imaging modality for distinguishing structural properties of the ACL in relation to adjacent musculoskeletal structures (7–10). Several multi-grading scoring systems have been developed to standardize reporting of knee joint abnormalities using MRI (11,12). The Whole-Organ Magnetic Resonance Imaging Scale (WORMS) is one of the most widely used semi-quantitative MRI scoring system for knee OA assessment (13–15) and considers a number of chondral, bony, and ligamentous compartments in the knee (15,16). The more recent Anterior Cruciate Ligament OsteoArthritis Score (ACLOAS) has been shown to offer increased longitudinal and cross-sectional reliability of ACL staging (17). The aforementioned grading metrics among others, however, are susceptible to inter-rater variability, especially pertaining to torn fibers and mucoid degeneration (10,18).

Deep learning methods have recently shown potential to serve as an aid for the clinician with limited time or experience in OA grading of the knee menisci and cartilage (9). Four other applications of deep learning have also resulted in binary models for distinguishing intact ACL from fully torn ACL (19–22). These neural networks possess large domains for learning, are versatile for new tasks using pre-trained weights, and can produce inferences in seconds. The specific mode of learning depends on the architecture, but the most successful algorithms are known to learn shallow features, as well as high-level features with many convolutions (23,24). To date, however, deep learning has yet to be applied to predict multi-grade, semi-quantitative lesion severity for the ACL.

In this study, we propose a deep learning based pipeline to isolate the ACL region of interest in the knee, detect ACL abnormalities, and stage lesion severity using novel three-dimensional (3D) and previously reported two-dimensional (2D) convolutions in MRIs. This is a proof-of-concept study to show that hierarchical image analysis methods work with 3D CNNs with the goal of hierarchical staging and comparison with the state-of-the-art 2D network. Additionally, to the best of our knowledge this is the first instance of multi-class ACL severity staging using deep learning, in which reconstructed, fully torn, partially torn, and intact ACLs are graded in accordance with semi-quantitative scoring. This deep learning pipeline would lend towards standardization and generalizability in assessing ACL lesions for clinicians with limited time or those with limited experience reading knee MRIs.

2 Materials and Methods

This work was sponsored by XX and XX. The funders had no editorial input into the project, and the authors had full control of the data.

2.1 Dataset

A total of 1243 knee MRI studies (224 unique subjects) were obtained from three prior research studies aimed to study joint degeneration in OA and after ACL injury. Subjects were excluded based on concurrent use of an investigational drug, history of fracture or total knee replacement in the study knee, and any contraindications to MR. Subjects were recruited in the OA group if they reported knee pain, aching, or stiffness on most days per month during the past year, use of medication for knee pain on most days per month during the past year, or any possible radiographic sign of knee OA (Kellgren-Lawrence (KL) >0), and age >35 years. Subjects were included in the control group if no knee pain or stiffness in either knee or use of medications for knee pain in the last year were reported, and if no radiographic evidence of OA on either knee was noted (KL=0).

Subjects in the ACL study were collected at three sites: _____. ACL patients underwent anatomic single-bundle ACL reconstruction by board-certified, fellowship-trained orthopedic surgeons. Only soft tissue grafts were used: hamstrings, either allograft or autograft, or posterior tibialis allograft. No special sequences were used for metal artifact suppression. Hamstring, patella tendon, and allograft ACL reconstructions typically do not cause metal artifacts along the intra-articular course of the graft and allow evaluation of ACL graft degeneration or re-tears. Moreover, metal artifacts related to ACL reconstruction are related to the use of metallic interference screws or Endobuttons, though many reconstructions typically make use of non-metallic interference screws and have no associated artifact. All patients underwent a standard postoperative rehabilitation protocol. Mean and standard deviation (SD) of age and body mass index (BMI) of subjects were 46.50 ± 13.55 and 24.58 ± 3.60 kg/m², respectively. Proportion of women was 46% .

The study was conducted according to regulations from the Committee for Human Research at all institutions, and all subjects provided informed consent. In all imaging studies from all three sites, 3D FSE CUBE proton density-weighted sagittal oblique sequences with the following parameters were used: repetition time / echo time = 1500 / 26.69 msec, field of view = 14 cm, matrix = 384 x 384, slice thickness = 0.5 mm, echo train length = 32, bandwidth = 50.0 kHz, number of excitations = 0.5, acquisition time = 10.5 min. All images were acquired with 3T MRI scanners (GE Healthcare, Waukesha, WI) and 8 surface coils.

Between 2011 and 2014, five board-certified radiologists (each with over 5 years of training) graded a non-overlapping section of the dataset. The radiologists were masked with respect to both number and type of lesion. An intra-observer agreement assessment was conducted by three additional board-certified radiologists currently involved with the study. All readers were trained by one senior radiologist who read at least 20 imaging studies with each of the other two radiologists in two imaging sessions. During these readings, the radiologists were explained both WORMS and ACLOAS gradings and they were asked to grade lesions of cartilage, menisci, bone marrow, ligaments and synovium under supervision with direct feedback. This training was followed by independent assessment of 60 randomly chosen cases from the dataset. The ACL was graded using the original WORMS grading scale. The WORMS grade was then placed into four classes including intact (grade 0), partial tear (grade 1), full tear (grade 2), and reconstructed (grade 3) in order to generalize newer ACL scoring systems (i.e. ACLOAS) for use in the deep learning pipeline. The linear weighted kappas for inter-reader agreement among each pair of the three radiologists were 0.66-0.78 for the ACL grading. The distribution of partial tears was small compared to that of full tears because the inclusion criteria in one of the studies was presence of fully torn ACL.

2.2 Deep Learning Pipeline

Our framework consists of a deep learning segmentation that categorizes the knee into 11 distinct anatomical components (24), followed by an image cropping to isolate the ACL, and a 3D CNN (convolutional neural network) to classify lesion severity (9) (**Figure 1**). The CNN was developed through a hierarchical approach; specifically, three cascaded models were built to classify: reconstructed ligaments, full tears, partial tears, and intact ACLs. We further compared the hierarchical approach to a single four class model with the same parameters, and saw superior performance using the hierarchical approach. The same hierarchical classification network was implemented with a 2D CNN for comparison with the 3D CNN (25).

2.3 ACL Localization

Two VNet architectures localized the volume of knee that included ACL; each VNet consisted of four down-sampling convolutions to learn an encoding for the volume, followed by four upward-convolutions to decode the segmentation mask (25). The VNet segmentation is a portion of a larger project aimed towards segmenting all knee tissues, which we used to isolate the ACL region of interest.

The first VNet segmented the patellar cartilage, femur, tibia, and meniscus from the image background. These five compartments were further segmented by a second VNet into 11 compartments consisting of patellar cartilage, medial and lateral femoral condyles, medial and lateral tibial cartilage, tibia, four meniscal horns, and background.

The VNets were trained and tested on a total of 480 manual segmentations. Rotations between -5 and 5 degrees were applied to augment the segmentations. All parameters of the originally published VNet were maintained, with the exception of the residual connections (25). The VNet was trained for 100 epochs using the following parameters: 10^{-5} learning rate, batch size of 1, Adam optimizer, with combined weighted cross entropy and Dice loss functions. This combined loss function enables increased penalization when the meniscus or cartilage are misclassified as background, mitigating the relatively small proportions of these two compartments in the entire knee.

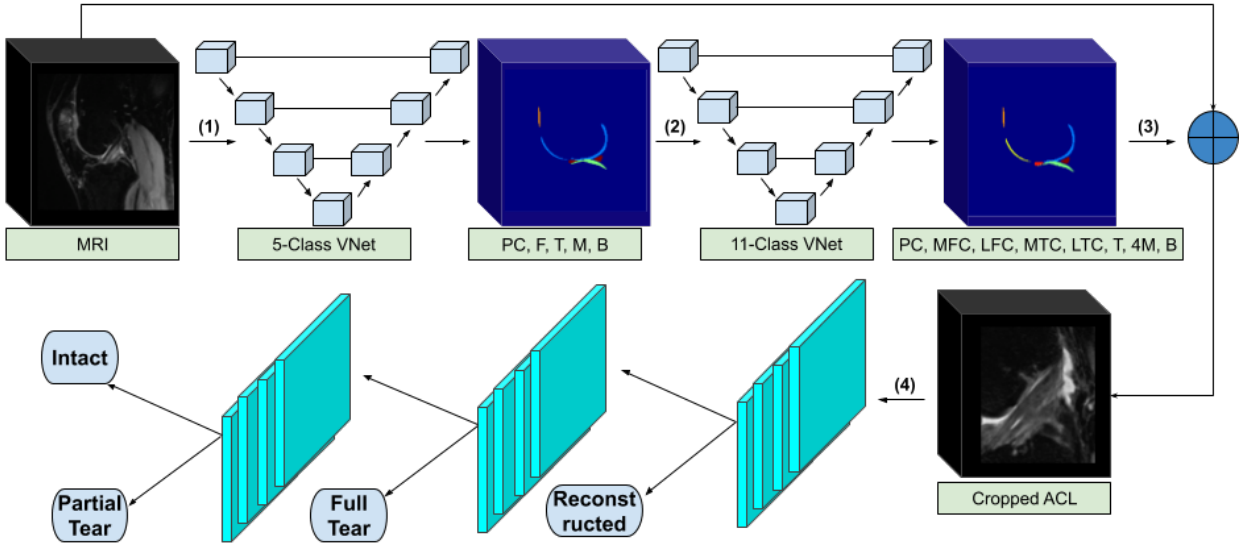


Figure 1: The segmentation and classification pipeline begins with (1) the input of a full MR volume into a 3D VNet which segments the knee into patellar cartilage (PC), femur (F), tibia (T), meniscus (M), and background (B). (2) The 5-class segmentation is then input to a second VNet which further categorizes the knee into 11 compartments including patellar cartilage (PC), medial and lateral femoral and tibial condyles (MFC, LFC, MTC, LTC), and four meniscal horns (4M). (3) The 11-class segmentation is used to determine the ACL boundaries of the original input MRI. (4) The cropped ACL volume is input to three hierarchical CNNs (either 2D or 3D), which each detect reconstructed, fully torn, partially torn, and intact ACLs.

To avoid any additional manual annotation, the femoral and tibial cartilage masks generated by the concatenated V Nets were then used to create bounds on the original knee MRI and isolate the ACL. Specifically, the ACL’s superior bound was determined by the superior point of the femoral condyle, inferior bound by inferior point of tibial cartilage, anterior bound by anterior point of tibial cartilage, posterior bound by posterior point of femoral cartilage, medial bound by medial point of femoral condyle, and lateral bound by medial point of lateral femoral condyle. All bounded ligament volumes were resized to the mean calculated volume of $98 \times 82 \times 47$ pixels³, and left knees were axially mirrored to match right knee orientation. We further calculated the intersection over union between manually segmented and automated VNet bound ACL regions in order to quantify the metric of overlap between clinical and deep learning segmentation. A random sample of 17 ACL volumes resulted in a mean(SD) intersection over union of 0.89(0.06).

2.4 Classification

2.4.1 3D CNN

The cropped ACL volumes were input into a CNN consisting of 3D convolutional kernels (9). The network is built with six layers, including one skip connection after the first convolution, to preserve initial features and mitigate overfitting (**Figure 2**). Training was performed over 100 epochs with the following parameters: an Adam optimizer, a learning rate of 10^{-5} , empirically weighted cross-entropy loss to account for class imbalances, and a batch size of 8. Three-dimensional translations and zooming were applied to all classes for augmentation of the training set. Rotations were not applied in order to preserve ligament fiber angles for model learning.

2.4.2 2D CNN

Performance of the 3D CNN was compared with the MRNet, a state-of-the-art 2D CNN (19). In the MRNet, each slice of the input 3D volume is passed through an AlexNet to extract features (26) (**Figure 3**). The MRNet was pre-trained on the ImageNet dataset, and additionally trained with the same training sets as the 3D CNN using transfer learning. The MRNet pools features within each slice and among all slices in the volume to produce a classification probability. The same image augmentations and loss functions as the 3D CNN were used to ensure correct comparison.

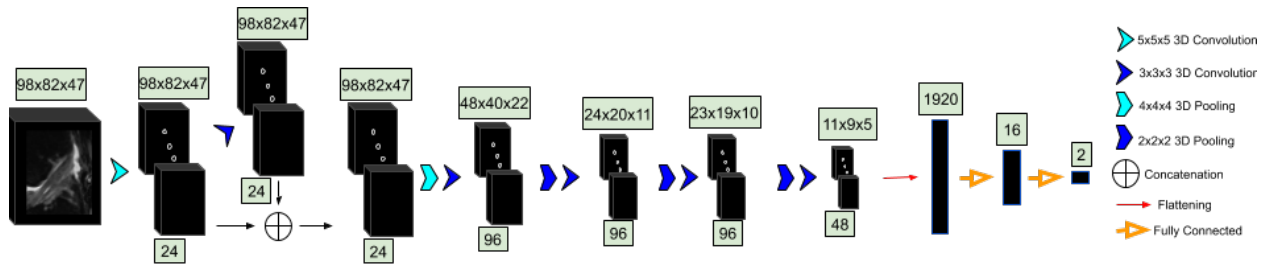


Figure 2: The MRI is input to the 3D CNN. In the first layer, convolutional kernels are applied to the entire volume. The second layer contains a concatenation with the first, followed by four additional 3D convolutions. The convolutional output is then flattened and input to two dense layers. The number beneath each set of blocks denotes the number of convolutions applied to the input; the number above represents the dimensions of the output after convolving the input.

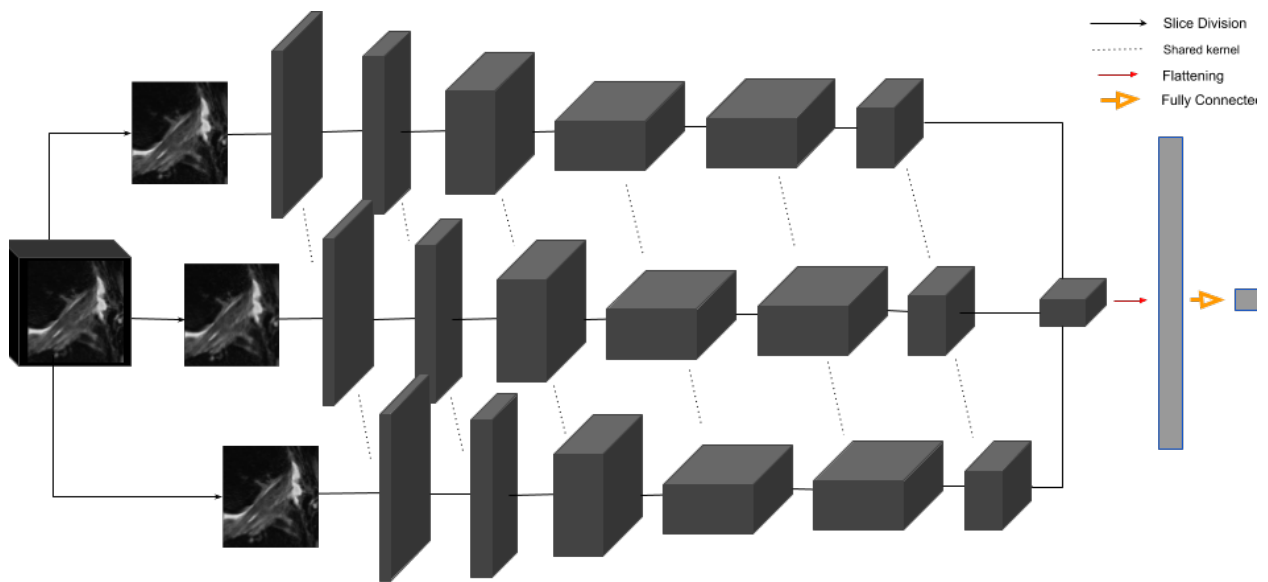


Figure 3: The 2D CNN, MRNet, feeds each slice of an MRI into an AlexNet with shared parameters across each kernel. The weights are pooled as they pass into a final convolution and a subsequent fully dense flattening layer. The output of the dense layer is a single probability for the input MRI. The full parameters of the architecture are reported by Bien et al (19).

2.5 Learning Strategy

The deep learning classifier first differentiated the reconstructed ligaments (grade 3) from grades 0-2. The remaining cases were then analyzed for detecting full thickness tears (grade 2). Partial tear lesions (grade 1) were further classified apart from intact ligaments (grade 0).

The total of 1243 images (1008 control, 235 injured) from 224 patients were split into train/validation/test sets (70%/10%/20%) for each grade, preserving the distributions of age, gender, and BMI. The studies in each split were from distinct, non-overlapping patients. There were no statistically significant differences between patients in the train, validation, and test sets regarding age ($p=.24$), BMI ($p=.17$), or gender ($p=.85$).

The 3D CNN was developed in Tensorflow (Google, Mountain View, CA), and the 2D CNN in Pytorch (Facebook, Menlo Park, CA). All computations were performed on NVIDIA (Santa Clara, CA) GeForce GTX Titan X graphics processing units.

2.6 Statistical Analysis

The training set was used to train each of the CNNs with back propagation. The validation set served to evaluate model performance at each training epoch, and the testing set was blind to the model until after training to serve as final metric of performance. For each CNN, we report overall accuracy and linear-weighted Cohen’s kappa (27), as well as sensitivity and specificity for each severity score. Model results were bootstrapped 100 times to obtain confidence intervals for each model’s performance on the testing set including sensitivity, specificity, accuracy, and linear-weighted Cohen’s kappa. Two-sample t-tests determined statistical significance between the two classifiers. We additionally paired ACLs from the testing set to analyze covariance with the McNemar test. P-values less than .05 were considered significant.

3 Results

The 3D CNN and 2D CNN had overall accuracies (mean(SD)) of 82(4)% and 84(4)% ($p=.005$), and linear-weighted kappas of .88(.02) and .92(.02) ($p<.001$), respectively. **Table 1** displays the distribution of grades for model training, while **Table 2** contains the total grades and demographics for the training, validation, and test sets. As seen in **Figure 4**, both models performed highest on reconstructed ACL classification. The 2D CNN demonstrated higher sensitivity and specificity in detecting intact ACLs (**Table 3**). The sensitivity of the 2D CNN in reconstructed ACLs was higher than that of the 3D CNN. The specificities in reconstructed classification were not significantly different. The McNemar test for covariance resulted in no significant differences between 2D and 3D CNNs for paired ACLs among each of the four severity stages and overall.

Table 1: Distribution of severity gradings in training set and groupings for each of the hierarchical neural network classifiers. Numbers within parentheses are image count and column wise percentage. Abbreviations: reconstructed (RCN), full tear (FT), partial tear (PT), intact (I).

Classifier Type	Reconstructed	Full Tear	Partial Tear
Negative Class	FT, PT, I (766/862, 88.9%)	PT, I (714/766, 93.2%)	I (702/714, 98.3%)
Positive Class	RCN (96/862, 11.1%)	FT (52/766, 6.8%)	PT (12/714, 1.7%)

Table 2: Distribution of ACL gradings in 224 patients.

Characteristic	Training Set	Validation Set	Test Set
Age mean(SD)	48.05 (12.84)	44.77 (16.31)	42.98 (13.50)
BMI mean(SD)	24.28 (3.52)	25.06 (3.95)	25.18 (3.61)
Women	83/146 (56.9%)	13/26 (50.0%)	25/52 (48.1%)
Intact	702/862 (81.4%)	103/127 (81.1%)	203/254 (79.9%)
Partial Tear	12/862 (1.4%)	2/127 (1.6%)	4/254 (1.6%)
Full Tear	52/862 (6.0%)	8/127 (6.3%)	17/254 (6.7%)
Reconstructed	96/862 (11.1%)	14/127 (11.0%)	30/254 (11.8%)

Table 3: Sensitivity and specificity for 3D and 2D CNNs in hierarchical severity staging of ACL injuries. Values reported in mean(SD).

Severity	3D Sensitivity	2D Sensitivity	P-Value	3D Specificity	2D Specificity	P-Value
Intact	.89(.02)	.93(.02)	<.001	.88(.04)	.90(.04)	<.001
Partial Tear	.74(.25)	.26(.25)	<.001	.92(.02)	1.00(.00)	<.001
Full Tear	.77(.10)	.83(.09)	<.001	1.00(.00)	.94(.02)	<.001
Reconstructed	.97(.03)	1.00(.00)	<.001	1.00(.00)	1.00(.00)	.40

Figure 5 displays a knee with intact ACL that was input into the pipeline, followed by localization of the ACL and the corresponding saliency map generated by the model’s classification weighting. Saliency maps were generated from the 3D CNN’s rectified linear unit output in its last dense layer. This ACL was correctly classified and possesses a high intensity on the inferior portion of the ligament’s saliency. An incorrectly classified intact ACL, predicted to be partially torn, is seen in **Figure 6**. The model placed a high intensity on a sagittal view with overlapping ACL and femur signal. The resulting saliency possessed large weight on a portion of the joint posterior to the ligament and also has speckles of noise further posterior. The 3D CNN took less than one second to classify a single ACL that went through all three hierarchical classifiers on one NVIDIA GeForce GTX Titan X graphics processing unit (12 GB).

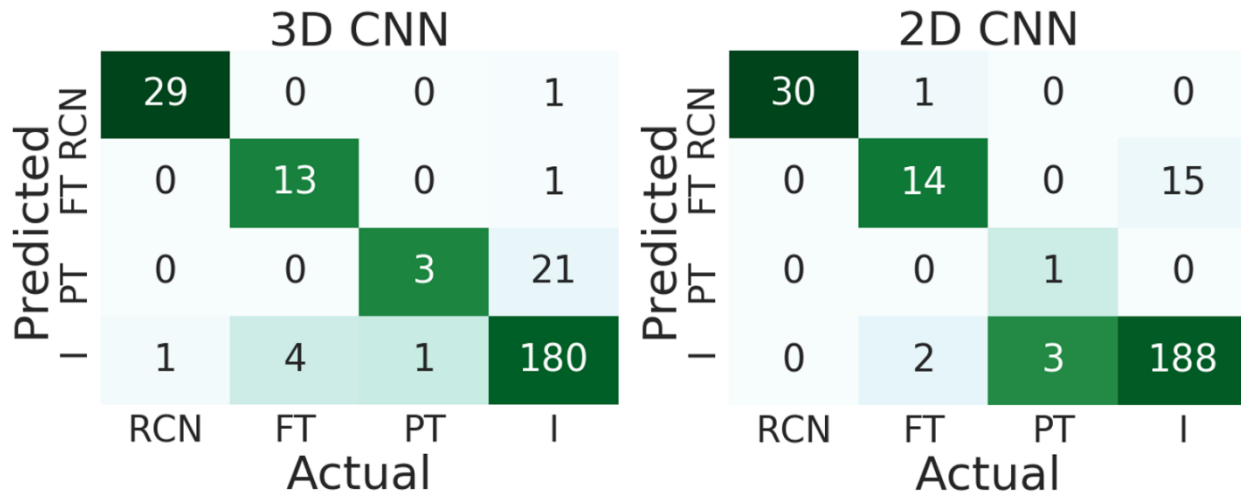


Figure 4: Confusion matrices for 3D and 2D CNNs of reconstructed (RCN), fully torn (FT), partially torn (PT), and intact (I) ACLs.

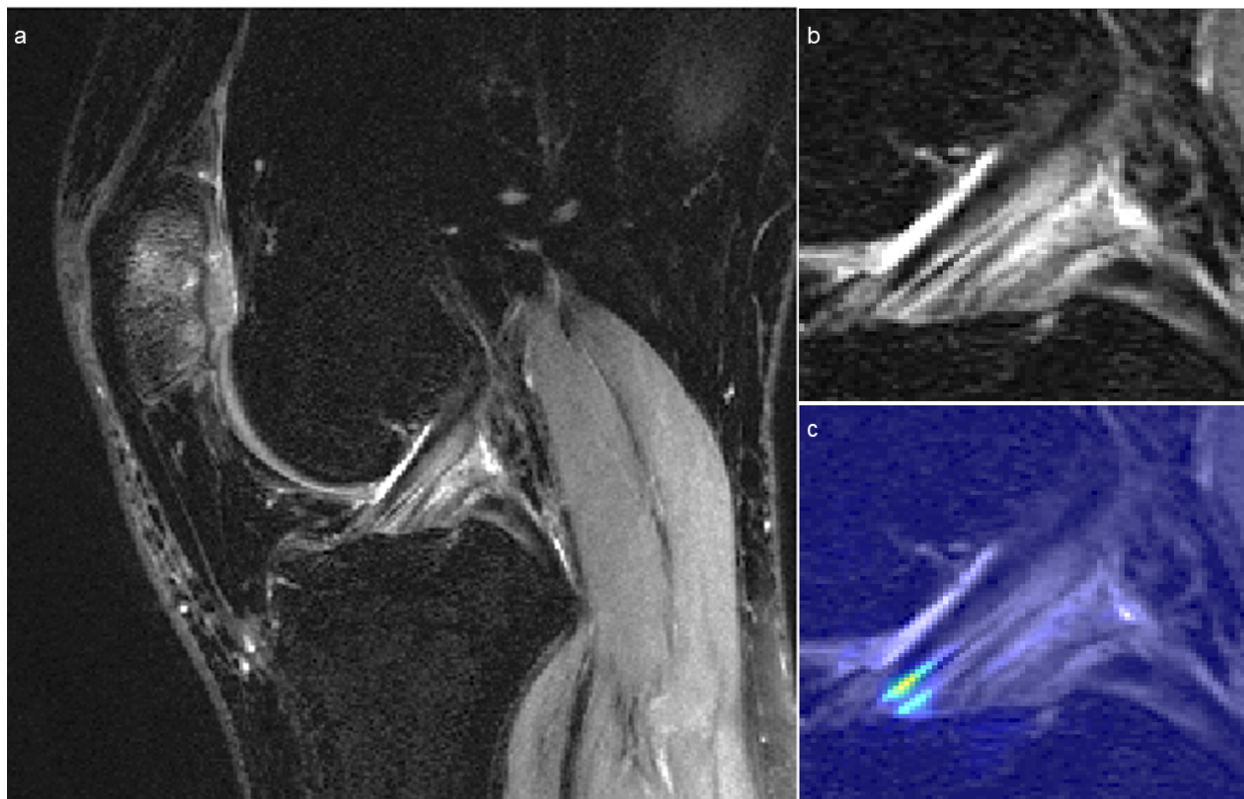


Figure 5: Sagittal views of (a) correctly classified knee with intact ACL and (b) its ACL localization with (c) overlaid saliency map. The saliency demonstrates the anterior-inferior portion of the ACL as high importance for model classification.

4 Discussion

In this work we present a fully-automated ACL segmentation and classification framework which provides hierarchical severity staging of the ACL using state-of-the-art deep learning architectures. We compare the performances of a 3D

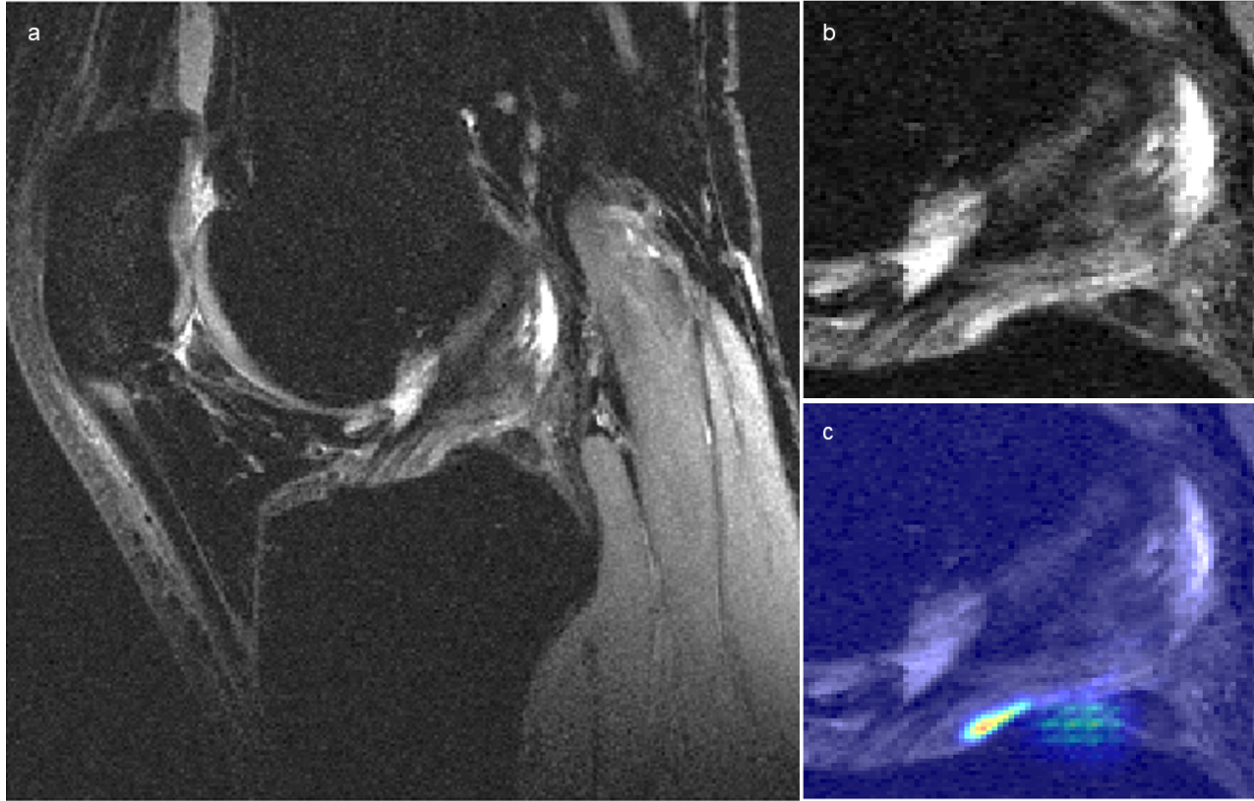


Figure 6: Sagittal views of (a) incorrectly classified knee with intact ACL and (b) its ACL localization with (c) overlaid saliency map. The model predicted a partial tear in this knee. The model misplaces a relatively high probability mapping on a slice with ACL that is obstructed by signal from femur. Additionally, the saliency intensity is posterior to the actual ligament; speckles of noise are also present in the inferior-posterior portion of the saliency. This intact ACL possessed focal fluid collection posterior to the ligament on a separate sagittal view, which may have led to the misclassification.

and a 2D CNN in ACL lesion classification. A higher overall accuracy and linear-weighted kappa were observed with the 2D model. This is the first reported fully automated segmentation and classification pipeline for multi-classification of the ACL in MRI.

Four previous groups have used deep learning frameworks for ACL lesion classification tasks, the first of which being the original MRNet by Bien et al (19). Their dataset consisted of 319 ACL tears from a total of 1,370 exams. Their MRNet displayed 97% sensitivity and 76% specificity for fully torn ACLs. The MRNet that we built, however, demonstrated a higher sensitivity than specificity. The discrepancy may be due to difficulty in generalizing the MRNet to images from other institutions. In addition, the difference may be due to transfer learning, through which the MRNet was trained with our unique dataset which tuned the original MRNet’s parameters.

Liu et al have approached the binary ACL tear classification task using three cascaded deep learning architectures: 1) LeNet performs slice selection to determine MRI slices possessing the ACL, 2) the You Only Look Once network performs a subsequent ligament isolation in the chosen slices, and 3) a Densenet detects the tears (28–30). The cascaded model achieved 96% in both sensitivity and specificity but was not statistically significant when compared to radiologist grading (20). In addition, this group used a relatively small number of images (350) for training, validation, and testing, which may have led to overfitting.

Chang et al applied CNNs with residual blocks for a third means of binary classification of torn and intact localized ACLs in MRIs. This study was conducted on 260 volumes in the coronal plane, which is a more difficult cross-section to use to grade the ACL (21). Most recently, Germann et al used CNNs to classify ACL tears in MRIs from 59 institutions, resulting in overall and in-house performance metrics lower than those of fellowship-trained faculty musculoskeletal radiologists (22).

Compared to these four prior studies, our pipeline classifies ACLs using 3D convolutional kernels in a hierarchical sequence. We implemented a hierarchical classifier because the ACLs possess an ordinal sequence of injury severity, increasing from intact to reconstructed. A stepwise approach beginning sequentially with the most severe classification can enhance accuracy because decisions are less complicated if binary. A true multi-class classifier would instead be warranted if categories had no relationships, such as differentiating among non-ordinal classes, while a linear regression would be necessary if severity increased on a continuous scale.

The hierarchical nature of our approach resulted in each individual severity stage in 2D and 3D possessing different cases based on upstream classifications. For example, the 3D reconstructed CNN predicted one fewer reconstructed ACL correctly compared to the 2D CNN. Thus, the subsequent full tear classifier in 3D possessed an additional reconstructed ACL to analyze. We utilized sensitivity and specificity measurements to interpret the performances of the individual classifier stages because the testing sets between 2D and 3D were inherently different. We additionally matched the testing images by ACL stage and performed the McNemar test to account for paired covariance between the 2D and 3D classifiers, resulting in no significant differences between 2D and 3D performance. However, this covariance statistic does not evaluate performance of each individual hierarchical classifier nor differentiate between incorrect classifications (i.e. staging a full tear as intact is not penalized more than staging a full tear as partial tear).

MRIs are 3D volumes and 3D convolutional kernels can learn 3D features that 2D convolutions cannot. The ground truth we are using is on the patient level on all the 3D volumes, which is a scalable design because it does not require pixel or slice level annotation. Thus, supervised feature learning can occur exclusively in 3D, as opposed to 2D. However, 3D models are more complex, higher parameter spaces that are more likely to overfit with small sample sizes, unlike 2D models which have lower parameter space convolutional filters and typically perform well for general image classification problems. Using a 3D CNN did not outperform a 2D model, which may be because the 2D CNN utilized transfer learning from ImageNet, which is a dataset of 14 million 2D images that is not compatible for training a 3D CNN. The pre-trained 2D CNN without transfer learning would perform worse had we not trained it with our MRIs. However, our goal was to compare transfer learning in a 2D CNN with a 3D CNN possessing no transfer learning, in order to compare the benefits of 3D spatial relations with those of transfer learning.

Upon interrogating other sagittal slices of the incorrectly classified ACL in **Figure 6**, we found extra-ligamentous ganglia or synovial cystic changes along the ACL, which are relatively frequent findings in clinical practice, to cause misclassification as ACL tear; this is explained by the fact that intra-ligamentous cysts are often seen with mucoid degeneration and partial ligamentous tears. If the ganglia are large enough and in very close proximity to the ligament, then the large fluid collections and the corresponding high signal can be a confounding factor that the model can incorrectly learn, leading to classifying intact ligaments as tears. While these are frequent findings in clinical practice, we had a limited number of such ganglia in our training dataset. A potential way to mitigate this error would be to not only increase the number of such cases but also manually segment ACLs in the next iteration of the model to isolate the ligament from extra-ligamentous features.

Although we evaluate a hierarchical severity staging classifier, the partial tear class has little clinical relevance without subcategorization because partial tears denote a wide spectrum of injury, some of which require surgery and others which do not. Our limited sample size of partial tears did not allow for sub-stratification, but one of the primary end goals of this study is to classify subcategories of partial tears ranging from intact to fully torn. The limited number of partial tears in validation and testing sets should be considered when externalizing the partial tear results, as many more cases are needed to draw significant conclusions. However, we believe the current study lays groundwork for moving closer to a clinically relevant severity staging adding upon previous binary classifications. The current addition of reconstructed and partially torn ACLs is presented as a proof-of-concept for the ability to automatize the severity staging of ACL with deep learning.

Our method contains several limitations beginning with the use of MRI as gold standard. The grades used for model training are dependent on subjective assessment by a radiologist. Crawford et al report 86.5% specificity and 95.2% sensitivity for ACL full tear classification with MR among board-certified radiologists (18), Phelan et al report 87% specificity and 93% sensitivity for full tear evaluation (31), and Lefevre et al found 95% specificity and 95% sensitivity for partial tear classification (32), underscoring variability in MR assessment of the ACL. Using arthroscopy as an additional standard of comparison may improve the ground truth labels for the ACLs, increasing the model's capability to learn accurately. However, the model learning is limited as early model building notably could not sub-classify mucoid degeneration within intact tears. Furthermore, our sample of patients was not balanced amongst all gradings, which we addressed by using a weighted cross entropy loss function during training for both 3D and 2D CNN models.

We split our dataset into training, validation, and testing sets according to patient. However, this may lead to correlations among multiple images from the same patient, which are non-independent observations. Despite this, accounting for such correlations in training neural networks is not common, as the majority of models are built using image augmentations to increase training capacity. Thus, even if each subject had solely one image, data augmentation would

yet lend towards correlation discrepancies. For this reason, dividing by images without preserving patient splits would offer little correlation benefit for the model, which would instead display falsely elevated accuracy by inferring on the same patients used for training.

The dataset was obtained from three studies with inclusion criteria such as full ACL tears and ACL lesions secondary to OA, which resulted in a heterogeneous sample relative to the general population of ACL lesions. Only one of the three studies possessed additional 2D FSE sequences for radiologist grading which may comparatively limit the observer grading accuracy in the other two studies. Additionally, the radiologists used only oblique sagittal sequences; using other planes would increase the validity of the grading. Future work should aim to obtain larger datasets to mitigate these imbalances and enhance external validity, with particular aim to include a wider age range since a noteworthy portion of our dataset were older and possessed later stages of OA and ACL injuries. This includes using images from different institutions obtained with other scanners and sequences. However, the study did utilize scanners from three separate locations that each had coil changes and several software upgrades over the course of the study period, which may lend towards model generalizability.

Deep learning can provide relatively fast classification and visualization of ACL lesions, which may facilitate clinical translation. CNNs may prove helpful for clinicians in training or without strong radiology backgrounds, particularly musculoskeletal, during acute settings where board-certified radiologists are not available or in circumstances where radiologist workload is high. Both CNNs evaluated in this study offer distinct benefits; a 2D CNN shows greater overall performance, while the 3D model without any transfer learning can learn more detailed features present in complex gradings. Both architectures displayed a relatively high degree of sensitivity and specificity for intact, fully torn, and reconstructed ACLs, which may warrant clinical value of deep learning as a tool for standardizing and generalizing ACL severity staging for clinicians with limited experience with knee MRI.

References

1. Spindler KP, Wright RW. Anterior cruciate ligament tear. *N Engl J Med. Mass Medical Soc*; 2008;359(20):2135–2142.
2. Johnston JT, Mandelbaum BR, Schub D, et al. Video analysis of anterior cruciate ligament tears in professional American football athletes. *Am J Sports Med. SAGE Publications Sage CA: Los Angeles, CA*; 2018;46(4):862–868.
3. Hunter DJ, Lohmander LS, Makovey J, et al. The effect of anterior cruciate ligament injury on bone curvature: exploratory analysis in the KANON trial. *Osteoarthr Cartil. Elsevier*; 2014;22(7):959–968.
4. Prodromos CC, Han Y, Rogowski J, Joyce B, Shi K. A meta-analysis of the incidence of anterior cruciate ligament tears as a function of gender, sport, and a knee injury–reduction regimen. *Arthrosc J Arthrosc Relat Surg. Elsevier*; 2007;23(12):1320–1325.
5. Brophy RH, Gill CS, Lyman S, Barnes RP, Rodeo SA, Warren RF. Effect of anterior cruciate ligament reconstruction and meniscectomy on length of career in National Football League athletes: a case control study. *Am J Sports Med. Sage Publications*; 2009;37(11):2102–2107.
6. Suter LG, Smith SR, Katz JN, et al. Projecting lifetime risk of symptomatic knee osteoarthritis and total knee replacement in individuals sustaining a complete anterior cruciate ligament tear in early adulthood. *Arthritis Care Res (Hoboken). Wiley Online Library*; 2017;69(2):201–208.
7. Shakoor D, Guermazi A, Kijowski R, et al. Cruciate ligament injuries of the knee: A meta-analysis of the diagnostic performance of 3D MRI. *J Magn Reson Imaging. Wiley Online Library*; 2019.
8. Ai T, Zhang W, Priddy NK, Li X. Diagnostic performance of CUBE MRI sequences of the knee compared with conventional MRI. *Clin Radiol. Elsevier*; 2012;67(12):e58–e63.
9. Padoia V, Norman B, Mehany SN, Bucknor MD, Link TM, Majumdar S. 3D convolutional neural networks for detection and severity staging of meniscus and PFJ cartilage morphological degenerative changes in osteoarthritis and anterior cruciate ligament subjects. *J Magn Reson Imaging. Wiley Online Library*; 2019;49(2):400–410.
10. Li K, Du J, Huang L-X, Ni L, Liu T, Yang H-L. The diagnostic accuracy of magnetic resonance imaging for anterior cruciate ligament injury in comparison to arthroscopy: a meta-analysis. *Sci Rep. Nature Publishing Group*; 2017;7(1):7583.
11. Hunter DJ, Guermazi A, Lo GH, et al. Evolution of semi-quantitative whole joint assessment of knee OA: MOAKS (MRI Osteoarthritis Knee Score). *Osteoarthr Cartil. Elsevier*; 2011;19(8):990–1002.
12. Brandt KD, Fife RS, Braunstein EM, Katz B. Radiographic grading of the severity of knee osteoarthritis: relation of the Kellgren and Lawrence grade to a grade based on joint space narrowing, and correlation with arthroscopic evidence of articular cartilage degeneration. *Arthritis Rheum. Wiley Online Library*; 1991;34(11):1381–1386.
13. Yang X, Li Z, Cao Y, et al. Efficacy of magnetic resonance imaging with an SPGR sequence for the early evaluation of knee cartilage degeneration and the relationship between cartilage and other tissues. *J Orthop Surg Res. BioMed Central*; 2019;14(1):152.

14. Hōng Z, Chen J, Zhang S, et al. Intra-articular injection of autologous adipose-derived stromal vascular fractions for knee osteoarthritis: a double-blind randomized self-controlled trial. *Int Orthop*. Springer; 2019;43(5):1123–1134.
15. Pēterfy CG, Guermazi A, Zaim S, et al. Whole-organ magnetic resonance imaging score (WORMS) of the knee in osteoarthritis. *Osteoarthr Cartil*. Elsevier; 2004;12(3):177–190.
16. Kretzschmar M, Lin W, Nardo L, et al. Association of physical activity measured by accelerometer, knee joint abnormalities, and cartilage T2 measurements obtained from 3T magnetic resonance imaging: data from the Osteoarthritis Initiative. *Arthritis Care Res (Hoboken)*. Wiley Online Library; 2015;67(9):1272–1280.
17. Rōemer FW, Frobell R, Lohmander LS, Niu J, Guermazi A. Anterior Cruciate Ligament OsteoArthritis Score (ACLOAS): longitudinal MRI-based whole joint assessment of anterior cruciate ligament injury. *Osteoarthr Cartil*. Elsevier; 2014;22(5):668–682.
18. Crawford R, Walley G, Bridgman S, Maffulli N. Magnetic resonance imaging versus arthroscopy in the diagnosis of knee pathology, concentrating on meniscal lesions and ACL tears: a systematic review. *Br Med Bull*. Oxford University Press; 2007;84(1):5–23.
19. Bien N, Rajpurkar P, Ball RL, et al. Deep-learning-assisted diagnosis for knee magnetic resonance imaging: development and retrospective validation of MRNet. *PLoS Med*. Public Library of Science; 2018;15(11):e1002699.
20. Liu F, Guan B, Zhou Z, et al. Fully Automated Diagnosis of Anterior Cruciate Ligament Tears on Knee MR Images by Using Deep Learning. *Radiol Artif Intell*. Radiological Society of North America; 2019;1(3):180091.
21. Chang PD, Wong TT, Rasiej MJ. Deep Learning for Detection of Complete Anterior Cruciate Ligament Tear. *J Digit Imaging*. Springer; 2019;1–7.
22. Germann C, Marbach G, Civardi F, et al. Deep Convolutional Neural Network–Based Diagnosis of Anterior Cruciate Ligament Tears: Performance Comparison of Homogenous Versus Heterogeneous Knee MRI Cohorts With Different Pulse Sequence Protocols and 1.5-T and 3-T Magnetic Field Strengths. *Invest Radiol*. 9000.
23. Cui Y, Song Y, Sun C, Howard A, Belongie S. Large scale fine-grained categorization and domain-specific transfer learning. *Proc IEEE Conf Comput Vis pattern Recognit*. 2018. p. 4109–4118.
24. Anumanchipalli GK, Chartier J, Chang EF. Speech synthesis from neural decoding of spoken sentences. *Nature*. Nature Publishing Group; 2019;568(7753):493.
25. Milletari F, Navab N, Ahmadi S-A. V-net: Fully convolutional neural networks for volumetric medical image segmentation. *2016 Fourth Int Conf 3D Vis*. IEEE; 2016. p. 565–571.
26. Krizhevsky A, Sutskever I, Hinton GE. Imagenet classification with deep convolutional neural networks. *Adv Neural Inf Process Syst*. 2012. p. 1097–1105.
27. Warrens MJ. Cohen’s linearly weighted kappa is a weighted average. *Adv Data Anal Classif*. Springer; 2012;6(1):67–79.
28. Han S, Pool J, Tran J, Dally W. Learning both weights and connections for efficient neural network. *Adv Neural Inf Process Syst*. 2015. p. 1135–1143.
29. Huang G, Liu Z, Van Der Maaten L, Weinberger KQ. Densely connected convolutional networks. *Proc IEEE Conf Comput Vis pattern Recognit*. 2017. p. 4700–4708.
30. Redmon J, Divvala S, Girshick R, Farhadi A. You only look once: Unified, real-time object detection. *Proc IEEE Conf Comput Vis pattern Recognit*. 2016. p. 779–788.
31. Phelan N, Rowland P, Galvin R, O’Byrne JM. A systematic review and meta-analysis of the diagnostic accuracy of MRI for suspected ACL and meniscal tears of the knee. *Knee Surgery, Sport Traumatol Arthrosc*. Springer; 2016;24(5):1525–1539.
32. Lefevre N, Naouri JF, Bohu Y, Klouche S, Herman S. Partial tears of the anterior cruciate ligament: diagnostic performance of isotropic three-dimensional fast spin echo (3D-FSE-Cube) MRI. *Eur J Orthop Surg Traumatol*. Springer; 2014;24(1):85–91.